(4)

MEMORANDUM REPORT BRL-MR-3662

(SUPERSEDES IMR-882)

BRL

1938 – Serving the Army for Fifty Years – 1988

COMPUTATIONAL STUDY OF THE M825 PROJECTILE WITH STANDARD AND DOME BASES

JUBARAJ SAHU
CHARLES J. NIETUBICZ
KAREN R. HEAVEY

MARCH 1986

U.S. ARMY LABORATORY COMMAND

BALLISTIC RESEARCH LABORATORY

ABERDEEN PROVING GROUND, MARYLAND

DESTRUCTION NOTICE

Destroy this report when it is no longer needed. DO NOT return it to the originator.

Additional copies of this report may be obtained from the National Technical Information Service, U.S. Department of Commerce, Springfield, VA 22161.

The findings of this report are not to be construed as an official Department of the Army position, unless so designated by other authorized documents.

The use of trade names or manufacturers' names in this report does not constitute indorsement of any commercial product.

DESTRUCTION NOTICE

Destroy this report when it is no longer needed. DO NOT return it to the originator.

Additional copies of this report may be obtained from the National Technical Information Service, U.S. Department of Commerce, Springfield, VA 22161.

The findings of this report are not to be construed as an official Department of the Army position, unless so designated by other authorized documents.

The use of trade names or manufacturers' names in this report does not constitute indorsement of any commercial product.

UNCLASSIFIED

SECURITY CLASSIFICATION OF THIS PAGE

REPORT DOCUMENTATION PAGE

Form Approved OMB No. 0704-0188

1a. REPORT SECURITY CLASSIFICATION: UNCLASSIFIED

1b. RESTRICTIVE MARKINGS:

2a. SECURITY CLASSIFICATION AUTHORITY:

2b. DECLASSIFICATION / DOWNGRADING SCHEDULE:

3. DISTRIBUTION / AVAILABILITY OF REPORT: Approved for public release, distribution unlimited.

4. PERFORMING ORGANIZATION REPORT NUMBER(S): BRL-MR-3662

5. MONITORING ORGANIZATION REPORT NUMBER(S):

6a. NAME OF PERFORMING ORGANIZATION: U.S. Army Ballistic Research Laboratory

6b. OFFICE SYMBOL (If applicable): SLCBR-LF-R

7a. NAME OF MONITORING ORGANIZATION:

6c. ADDRESS (City, State, and ZIP Code): Aberdeen Proving Ground, Maryland 21005-5066

7b. ADDRESS (City, State, and ZIP Code):

8a. NAME OF FUNDING / SPONSORING ORGANIZATION:

8b. OFFICE SYMBOL (If applicable):

9. PROCUREMENT INSTRUMENT IDENTIFICATION NUMBER:

8c. ADDRESS (City, State, and ZIP Code):

10. SOURCE OF FUNDING NUMBERS

PROGRAM ELEMENT NO	PROJECT NO.	TASK NO.	WORK UNIT ACCESSION NO.
61102A	1L161102AH43	00	001 AJ

11. TITLE (Include Security Classification): COMPUTATIONAL STUDY OF THE M825 PROJECTILE WITH STANDARD AND DOME BASES

12. PERSONAL AUTHOR(S): SAHU, JUBARAJ, NIETUBICZ, CHARLES J., and HEAVEY, KAREN R.

13a. TYPE OF REPORT	13b. TIME COVERED	14. DATE OF REPORT (Year, Month, Day)	15. PAGE COUNT
Memorandum Report	FROM _____ TO _____		

16. SUPPLEMENTARY NOTATION:

17. COSATI CODES			18. SUBJECT TERMS (Continue on reverse if necessary and identify by block number)		
FIELD	GROUP	SUB-GROUP	Transonic Flow	Base Cavity	
01	01		Implicit	Navier-Stokes	Drag Components
20	04		Recirculation	Base Flow	Axisymmetric

19. ABSTRACT (Continue on reverse if necessary and identify by block number)

Test firings of a 155mm artillery projectile have shown that its flight performance is affected by small changes in the base cavity configurations. A clear understanding of why these changes affect the flight behavior does not exist. A computational study has been made for the two base cavity configurations flight tested. Flowfield computations have been performed at $0.8 \leq \text{Mach} \leq 1.5$ using a Navier-Stokes base flow code. The aerodynamic drag components have been computed and the total drag determined. Computed results show differences in qualitative features of the recirculatory flow in the base region. The code predicts small differences in drag between the base cavity configurations.

20. DISTRIBUTION / AVAILABILITY OF ABSTRACT: ☐ UNCLASSIFIED/UNLIMITED ☐ SAME AS RPT ☐ DTIC USERS

21. ABSTRACT SECURITY CLASSIFICATION: UNCLASSIFIED

22a. NAME OF RESPONSIBLE INDIVIDUAL: Jubaraj Sahu

22b. TELEPHONE (Include Area Code): (301) 278-3707

22c. OFFICE SYMBOL: SLCBR-LF-R

DD Form 1473, JUN 86 — Previous editions are obsolete.

SECURITY CLASSIFICATION OF THIS PAGE

UNCLASSIFIED

TABLE OF CONTENTS

LIST OF FIGURES

I. INTRODUCTION

The ability to compute the base region flow field for projectile configurations using Navier-Stokes computational techniques has been developed over the past few years. This capability is most important for determining aerodynamic coefficient data and in particular the total aerodynamic drag. The total drag as described in this paper consists of the pressure drag (excluding the base), viscous drag and base drag components. At transonic and low supersonic speeds the base drag component is the major contributor to the total aerodynamic drag.

The majority of base flow calculations to date have modeled the base region as a flat solid surface. Many of the actual configurations have some form of base cavity. General opinion has been that the inclusion of a base cavity or modifications to the interior cavity of a projectile base would have little or no effect on the overall flight performance parameters.

The M825 projectile under certain conditions is expected to be aeroballistically similar to its parent configuration the M483A1. The M825 has an aluminum/steel base which is configured as a flat cavity (standard). A recent product improvement program, undertaken to reduce the production costs and improve shell integrity, resulted in the design of a new base configuration made from steel and containing a dome cavity. A series of aeroballistic tests[1] were conducted in the Transonic Range Facility of the US Army Ballistic Research Laboratory (BRL), to determine any difference in the aeroballistics which may occur between the standard and dome base configurations. As a result of these tests, differences in aerodynamic performance were found to exist between the two rounds. The most significant changes in the aerodynamic data were in the lift and static moment coefficients. The drag was found to be reduced by a few percent with the dome configuration having the lower drag.

A computational study was undertaken to determine the ability of the present Navier-Stokes codes to predict these differences and to further understand the fluid dynamic behavior which can account for such small changes. The use of Navier-Stokes codes can provide a detailed description of the flow field associated with the M825 configuration as well as the integrated aerodynamic coefficients. The work reported here has been accomplished using an axisymmetric base flow code. Numerical computations have been completed for a Mach number range of $0.8 \leq M \leq 1.5$. The computed aerodynamic drag show the same effect as the experimental data, that is, a small reduction in the total aerodynamic drag. Qualitative features of the computed flow field are presented in the form of mach contours and particle traces.

II. GOVERNING EQUATIONS AND SOLUTION TECHNIQUE

1. GOVERNING EQUATIONS

The complete set of time-dependent thin-layer Navier-Stokes equations is solved numerically to obtain a solution to this problem. The numerical technique used is an implicit finite difference scheme. Although time-dependent calculations are made, the transient flow is not of primary interest at the present time. The steady flow, which is the desired result, is obtained in a time asymptotic fashion.

The time-dependent, thin-layer, Navier-Stokes equations written in strong conservation law form for the axisymmetric formulation[2] are:

$$\frac{\partial \hat{q}}{\partial \tau} + \frac{\partial \hat{E}}{\partial \xi} + \frac{\partial \hat{G}}{\partial \zeta} + \hat{H} = \frac{1}{Re}\frac{\partial \hat{S}}{\partial \zeta} \quad . \tag{1}$$

The general coordinate transformations are defined as:

$\xi = \xi(x,y,z,t)$ is the longitudinal coordinate

$\eta = \eta(x,y,z,t)$ is the circumferential coordinate

$\zeta = \zeta(x,y,z,t)$ is the near normal coordinate

$\tau = t$ is the time.

The vector $\hat{q}$ contains the dependent variables [ρ, ρu, ρv, ρw, e] and the flux vectors $\hat{E}$, $\hat{G}$ contain terms which arise from the conservation of mass, momentum and energy in the three coordinate directions. The source vector $\hat{H}$, in Equation (1), contains terms which result from an analytic determination of the circumferential flux vector, given the assumption of axisymmetric flow and constant angular velocity.[2] The viscous terms are contained in the vector $\hat{S}$ which is seen to have variation in the ζ direction only. This is representative of the thin-layer approximation.

2. SOLUTION TECHNIQUE

Equation (1) is solved using the Beam and Warming[3] implicit approximately factored finite difference scheme which uses central differencing in both ξ and ζ directions. Code improvements have been made to include a variable time step, numerical smoothing based on local solution gradients and code vectorization.[4] The Beam-Warming implicit algorithm has been used in various applications[3-6] for the equations in general curvilinear coordinates. The algorithm is first-order accurate in time and second- or fourth-order accurate in space. The equations are factored (spatially split), which reduces the solution process to one-dimensional problems at a given time level. Central difference operators are employed and the algorithm produces block tridiagonal systems for each space coordinate. The main computational work is contained in the solution of these block tridiagonal systems of equations.

To suppress high frequency components that appear in regions containing severe pressure gradients e.g., shocks or stagnation points, artificial dissipation terms are added. In the present application, a switching dissipation model is used which is a blend of second- and fourth-order dissipation terms. This model uses a fourth-order dissipation in smooth regions and switches to a second-order dissipation in regions containing high pressure or density gradients. Incorporation of this dissipation model has resulted in an improvement in the quality of the results and has made the code more robust.

The developed axisymmetric code uses a unique flow field segmentation procedure to compute the full flow field over a projectile or a missile including the base region. This procedure preserves the sharp corner at the base. The details of this development can be found in Reference 6. For the computation of turbulent flows, the two-layer algebraic Baldwin-Lomax turbulence model[7] is used over the body. A second algebraic turbulence model which is based on a simple exchange-coefficient concept is used in the base region.[8]

III. MODEL GEOMETRY AND COMPUTATIONAL GRID

The external configuration of the M825, excluding the base, is similar to the M483A1 shown in Figure 1. The features of this projectile which have not been modeled exactly are the meplat on the fuze and the rotating band near the base. The rotating band was eliminated and the meplat was modeled as a hemisphere cap. The computational model is shown in Figure 2 and consists of a 2.84 caliber nose, a 2.7 caliber cylindrical section, and a 0.26 caliber 8° boattail. The ogive contours were matched as well as the undercut on the cylindrical section.

The current problem of interest is the effect of the different base geometries on the overall projectile aerodynamics. Figure 3a and 3b show the standard and dome base configurations respectively. The standard base is a combination of aluminum and steel and contains a base cavity which is characterized as a flat surface. The PIP configuration is an all steel base and is characterized as a domed surface. The cavity volume is also significantly larger for the dome configuration.

The solution technique requires the discretization of the entire flow region of interest into a suitable computational grid. The grid outer boundary has been placed at 2.5 body lengths upstream and surrounding the projectile. The downstream boundary was placed at 2 body lengths. Since the calculations are in the subsonic/transonic regime the computational boundaries must extend out beyond the influence of the body. This ensures that the boundary conditions specified in the flow code are satisfied.

Figure 4 shows a grid generated for the standard configuration. The grid consists of 225 points in the streamwise direction and 50 points in the normal direction. This is broken down into two sections: a body region and a base region. The surface points for each region are selected using an interactive design program. Each grid section is then computed separately using a hyperbolic grid generation program.[9] There are 165 points along the projectile surface, including 60 points along the afterbody. The normal distribution of points in base region consists of 50 points along the base cavity. Longitudinally, the base region is matched point for point with the 60 surface points on the afterbody. An expanded view of the base grid is shown in Figure 5a. The generally flat sections on the standard base enabled a grid to be routinely generated. However, due to the extreme concavity the grid for the dome base (Figure 5b) required an increase in the smoothing values used by the hyperbolic grid generator, as well as the addition of a grid averaging technique.

IV. RESULTS

Numerical computations have been made for both the standard and the dome base configurations for the range of Mach numbers from M = 0.80 to 1.5 and at zero angle of attack. Solutions were marched in time until the steady state results were achieved. Atmospheric flight conditions were used.

A few qualitative results are presented next. Figures 6 and 7 show the Mach number contours for the dome base configuration for M = 0.98 and 1.1, respectively. Figure 6 shows the flow expansion at the ogive corner, a shock-wave on the cylinder, and an expansion at the boattail corner. In addition, a shock system exists downstream of the base corner. As the Mach number is increased to 1.1, the flow pattern has changed. For this Mach number, Figure 7 shows a bow shock system in front of the nose of the projectile as well as the expansions at the ogive and boattail corners. The expansion at the base corner is much more pronounced and is followed by the recompression shock downstream of the base.

Figure 8 shows that the particle traces at Mach number, M = 1.1 and α = 0. It shows the flow expanding at ogive and boattail corners. In addition, the recirculatory flow in the base region is evident. The recirculation region extends to about one caliber downstream of the base corner. Expanded views of the particle trace plot in the base region are shown in Figures 9a and 9b, respectively, for the standard and dome base configurations. As shown in Figure 9a for the standard base, the back flow, upon reaching the cavity follows the contour of the cavity and leaves the cavity pushing the flow upwards. This, in turn, creates the secondary bubles seen near the base corner. The shear layer leaving the base corner is displaced upwards weakening the expansion at the base. It clearly shows the primary bubble and the secondary bubbles. Figure 9b shows the particle traces for the dome configuration. The flow again follows the contour of the cavity and upon leaving the dome cavity, is almost parallel to the streamwise direction. This flow, thus, has less effect on the free shear layer and doesn't weaken the expansion at the base corner as much compared to the standard base. The net effect is that the size of the primary bubble for the dome base is slightly smaller than that for the standard base. The reattachment point is therefore closer to the base and should result in lower base pressure or higher base drag.

Since the entire flowfield over the projectile including the base region is computed, all three drag components can be determined and thus, the total aerodynamic drag can be obtained. As stated earlier, solutions were marched in time until the steady state results were obtained. One of the ways to check for convergence is to look at the time history of the aerodynamic drag. Shown in Figure 10 is the time history for all the drag components as well as the total drag at M = 1.1 for the standard base. As seen here, the solution has converged in 2000 time iterations. The viscous drag and pressure drag components have converged in less than 500 iterations. However, as expected, it takes a lot longer for the base region flow to converge. The base flow is oscillating in the transient stage but the final converged result indicate that the flow is steady. This result is typical of the high transonic Mach number ($M > 1.1$) runs for both base configurations. At low transonic Mach numbers ($M < 1.1$), some unsteadiness in the flowfield has been observed. A typical plot for such a case is shown in Figure 11 for Mach = 0.8. As seen in this figure, the base drag as well as the pressure drag both indicate a

periodic unsteady flow behavior. The drag values for these cases have been taken as the averages of the amplitude extremes.

Figure 12 shows the pressure drag as a function of Mach number. The pressure drag rise in the transonic speed regime is clearly predicted. The difference in pressure drag between the two projectiles (standard base and dome base) is very small at high transonic Mach numbers and gets larger ($\approx 15\%$) at the low transonic Mach numbers ($M \approx 0.9$). The viscous drag component is shown in Figure 13. This component of the total drag is rather small and the difference in viscous drag due to the base configurations is negligible. The difference in the shapes of the cavities is expected to impact the base drag which is shown in Figure 14. The difference in base drag between the standard base and the dome base is larger at the high transonic Mach numbers ($1.1 \leq M \leq 1.5$) as well as at low transonic speeds ($M < 0.94$). The difference is very small near $M \approx 0.97$. In addition, the base drag is higher for the dome base than the standard base at high transonic Mach numbers ($0.97 \leq M \leq 1.5$) while the reverse is true at low transonic Mach numbers ($M < 0.97$). The expected rise in base drag at transonic speeds is clearly predicted. Comparison of the total aerodynamic drag is shown in Figure 15. As shown in this figure, the difference in drag is very small near $M \approx 0.97$ and is somewhat larger at high transonic speeds ($1.1 \leq M \leq 1.5$) as well as at low transonic speeds ($M < 0.92$). This plot also shows the range data for both base configurations. The overall comparison of the computed drag data with the range data is fair. As seen in the range data, the dome base has higher drag especially at higher transonic Mach numbers and this trend is seen in the computed results also.

V. CONCLUDING REMARKS

Numerical computations have been made for a projectile with two base cavity configurations at transonic speeds. Computed results show differences in the qualitative features of the base region flowfield between the two base cavities. The drag components and the total drag have been computed. Changes in the base cavity configuration have been found to affect the aerodynamic drag. Differences in drag of between 0 to 15% have been predicted. The dome base configuration produces a higher drag especially at higher transonic speeds ($1.1 \leq M \leq 1.5$) and qualitatively agrees with the trend of the experimental range data. At lower transonic speeds ($M < 0.97$), the reverse is true.

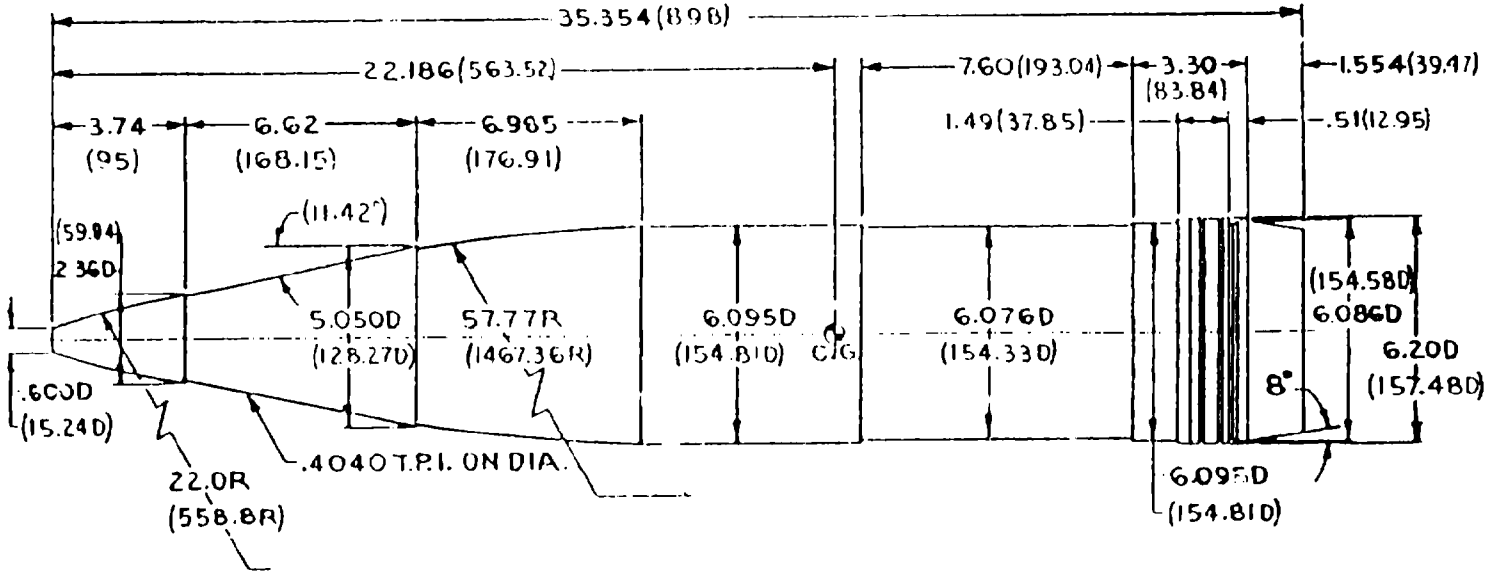

NOTE:-DIMS. ARE IN INCHES & MM( )

Figure 1. Actual XM825 projectile.

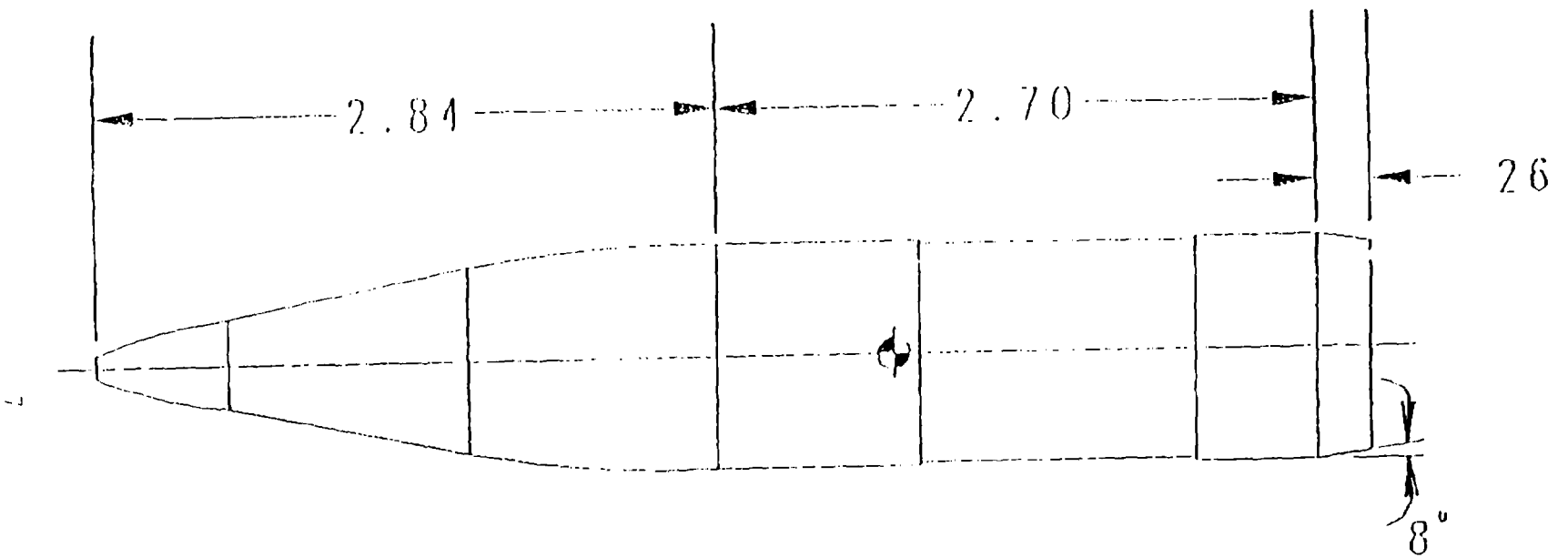

Figure 2. Computational model.

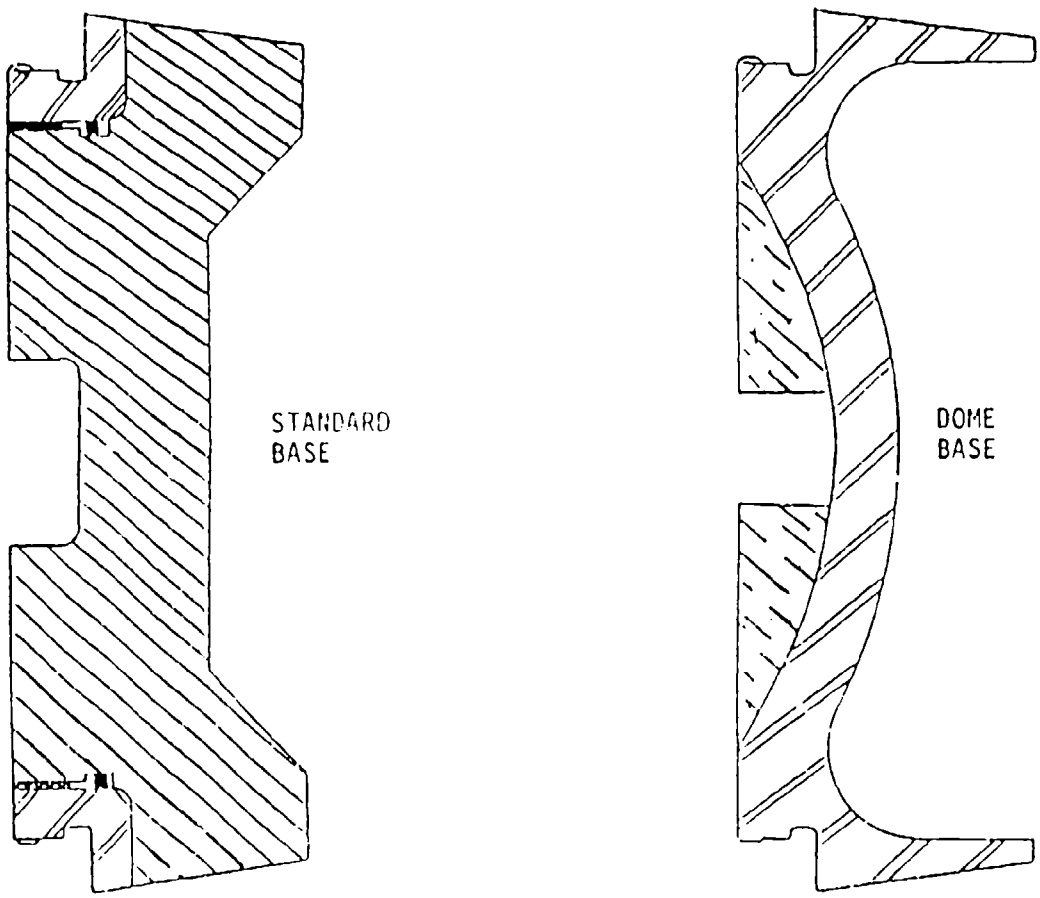

Figure 3. Base cavity configurations.

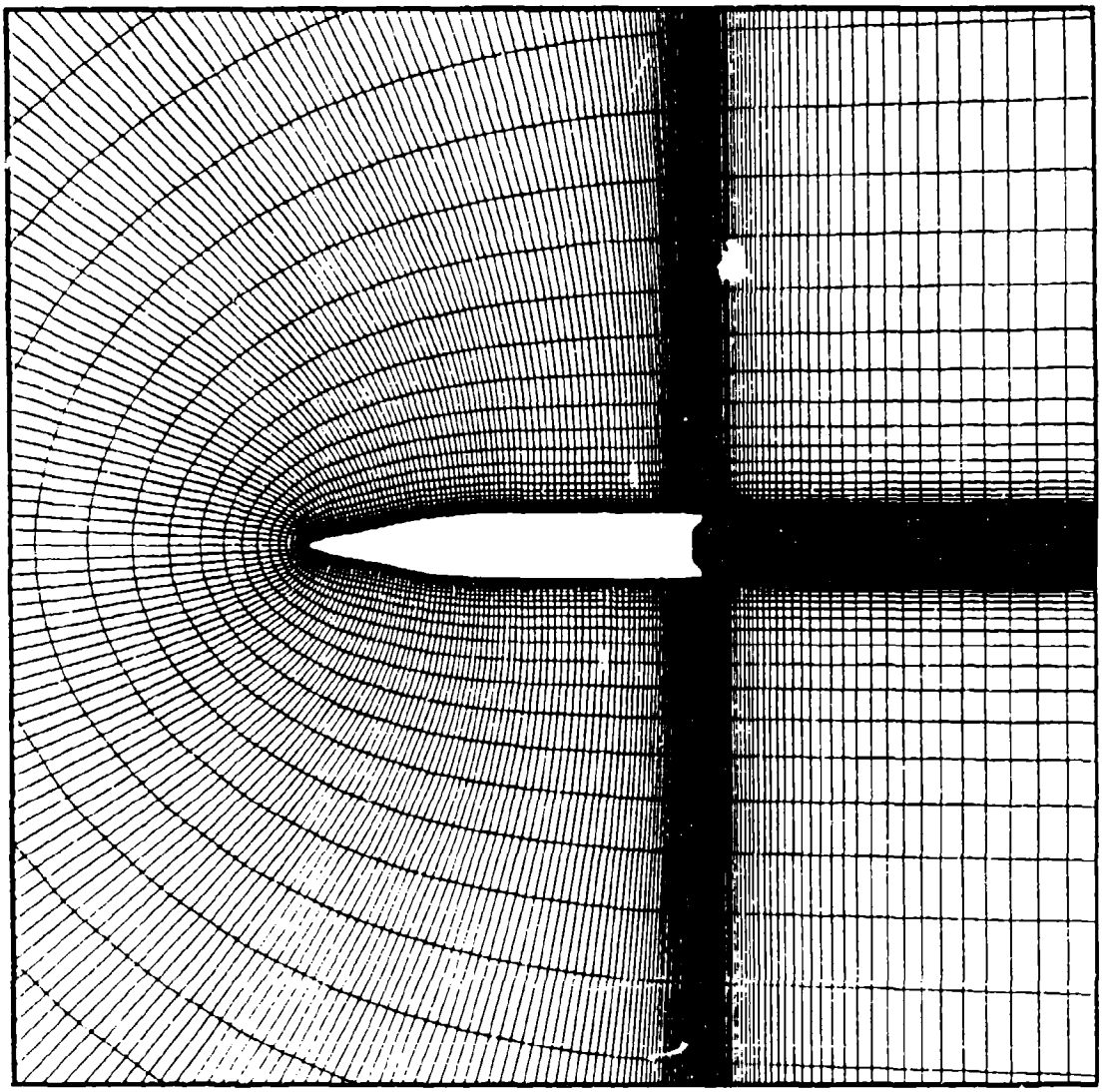

Figure 4. Computational grid expanded near the model.

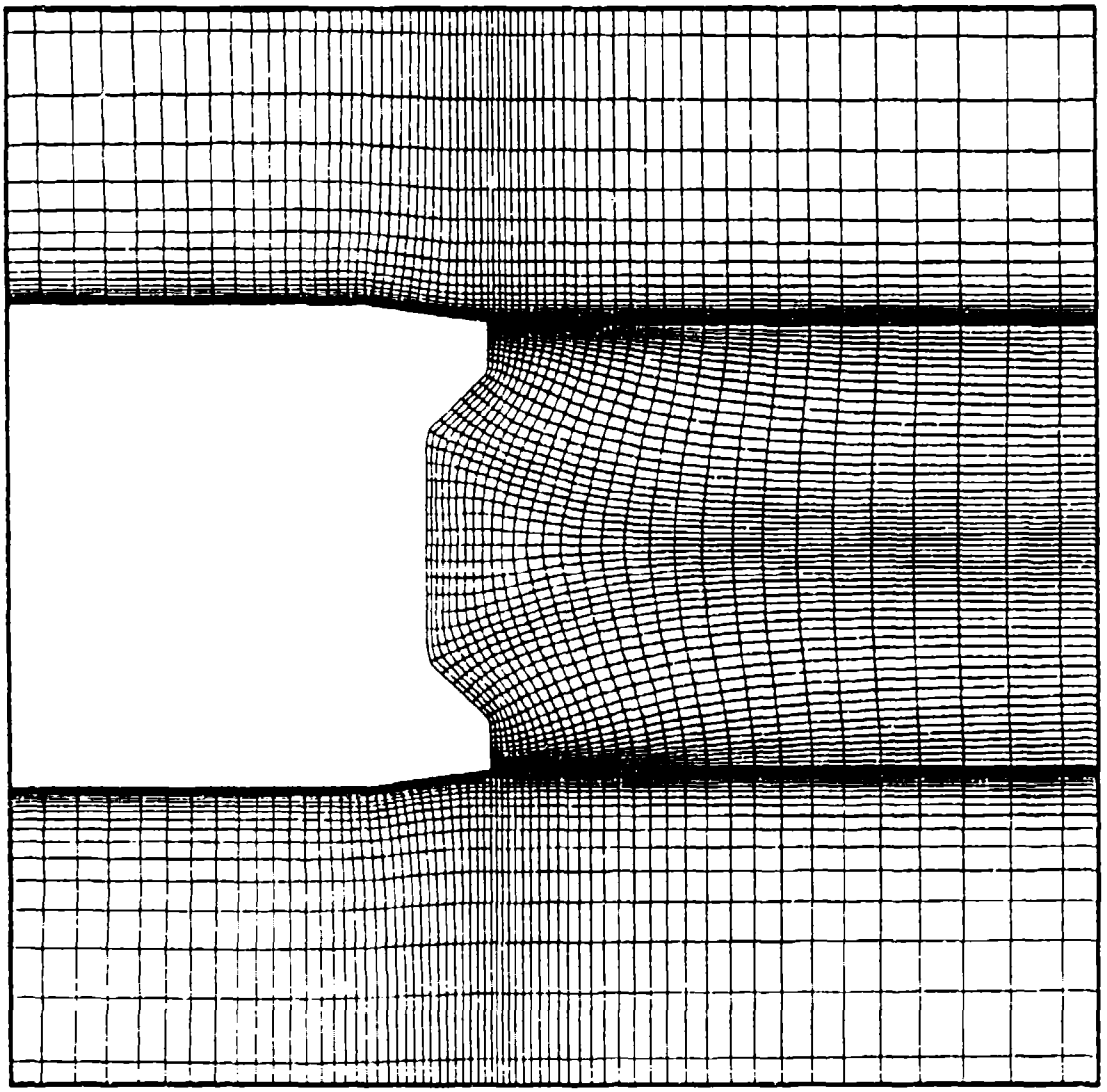

Figure 5a. Base region grid for the standard base.

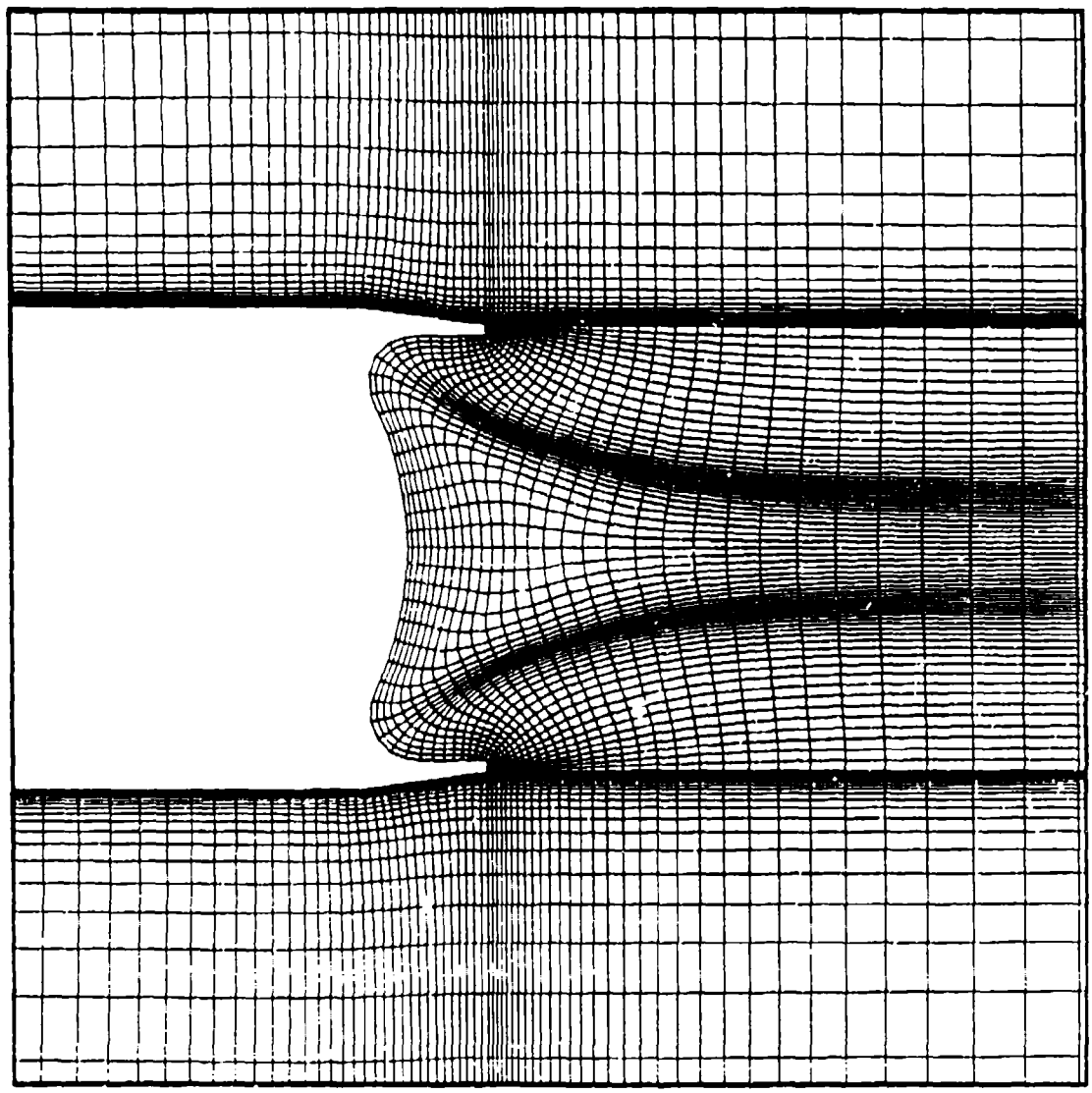

Figure 5b. Base region grid for the dome base.

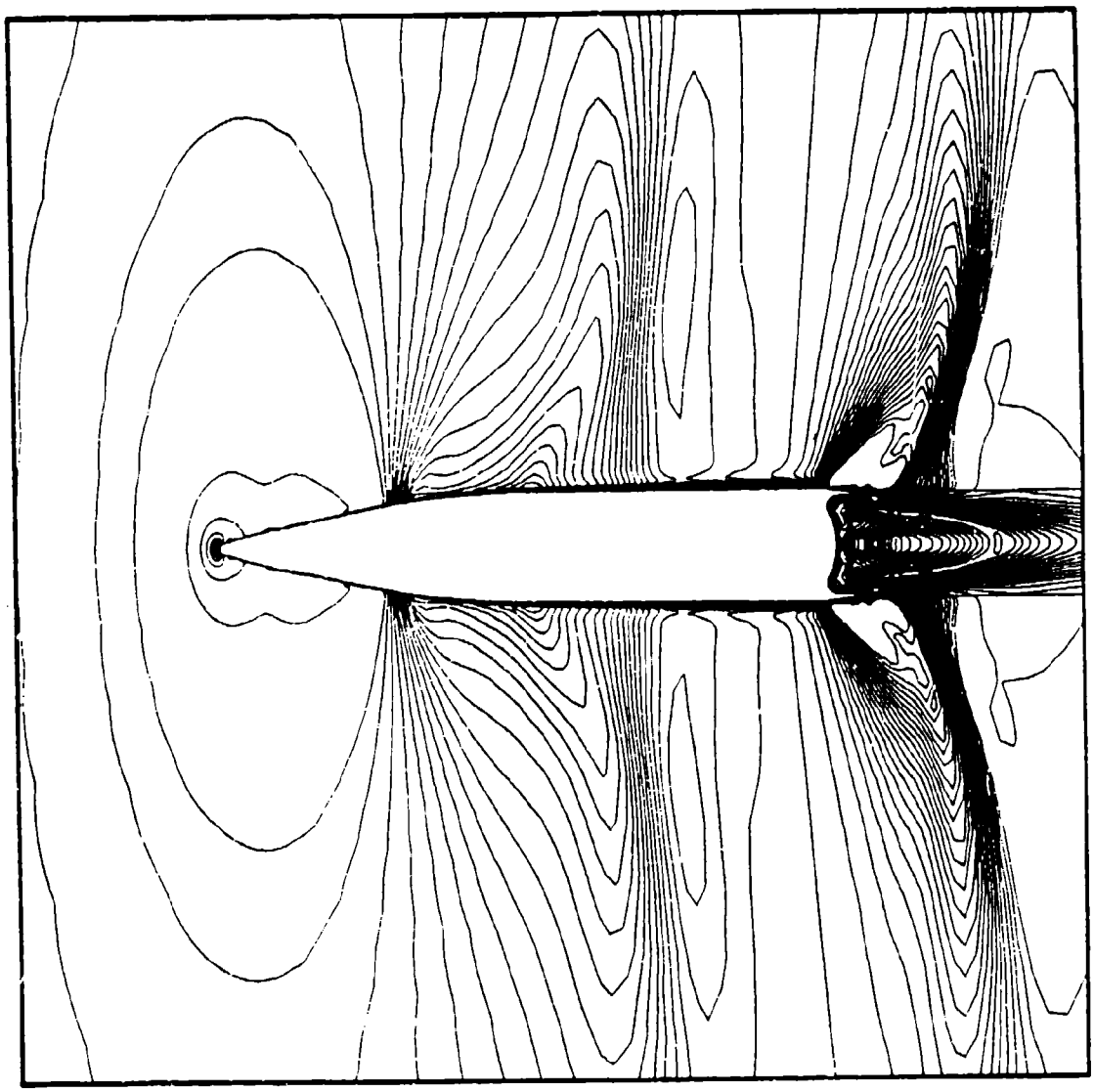

Figure 6. Mach number contours, $M_\infty = 0.98$, $\alpha = 0$, (dome base).

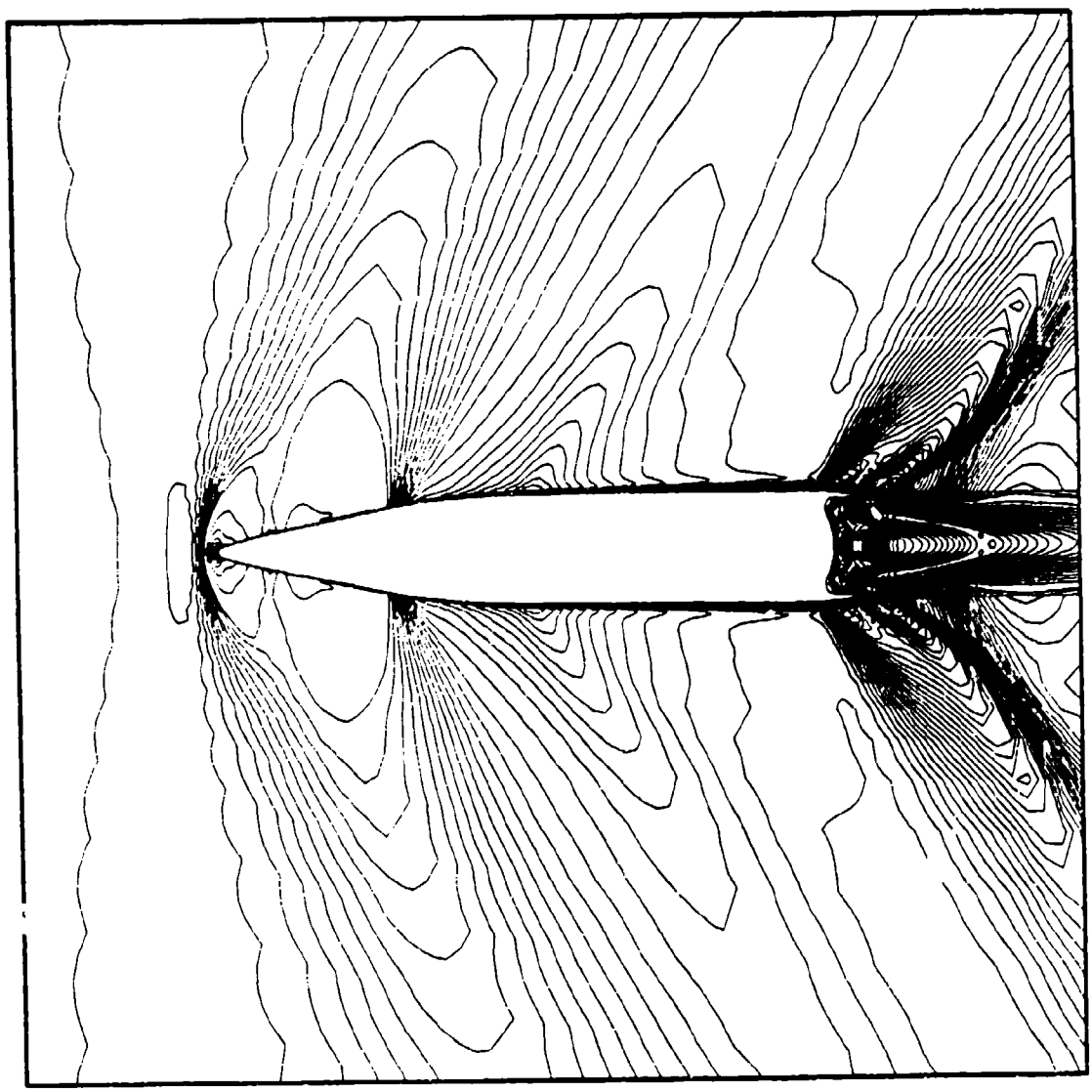

Figure 7. Mach number contours, $M_\infty = 1.1$, $\alpha = 0$, (dome base).

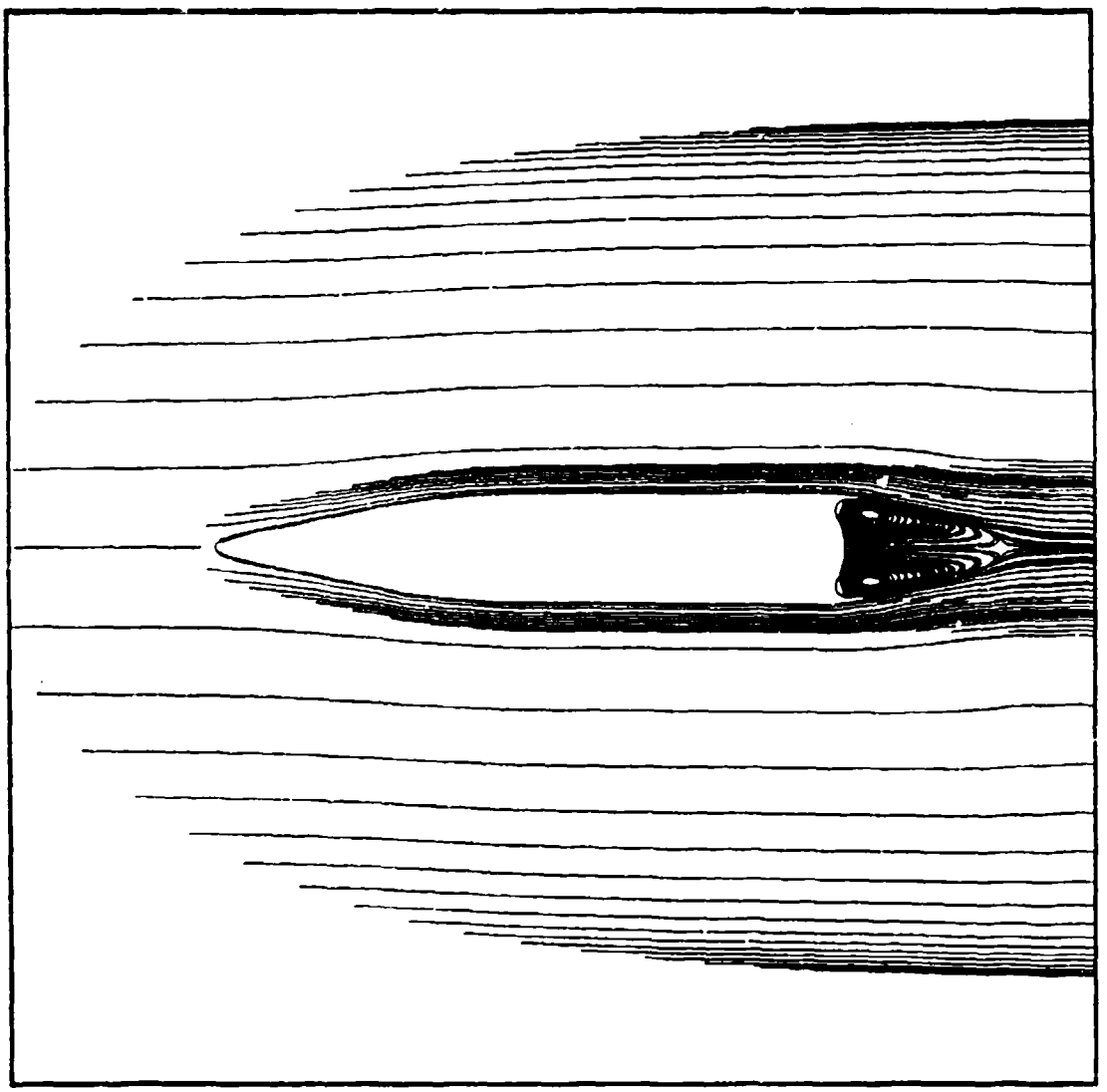

Figure 8. Particle traces over the projectile, $M_\infty = 1.1$, $\alpha = 0$, (dome base).

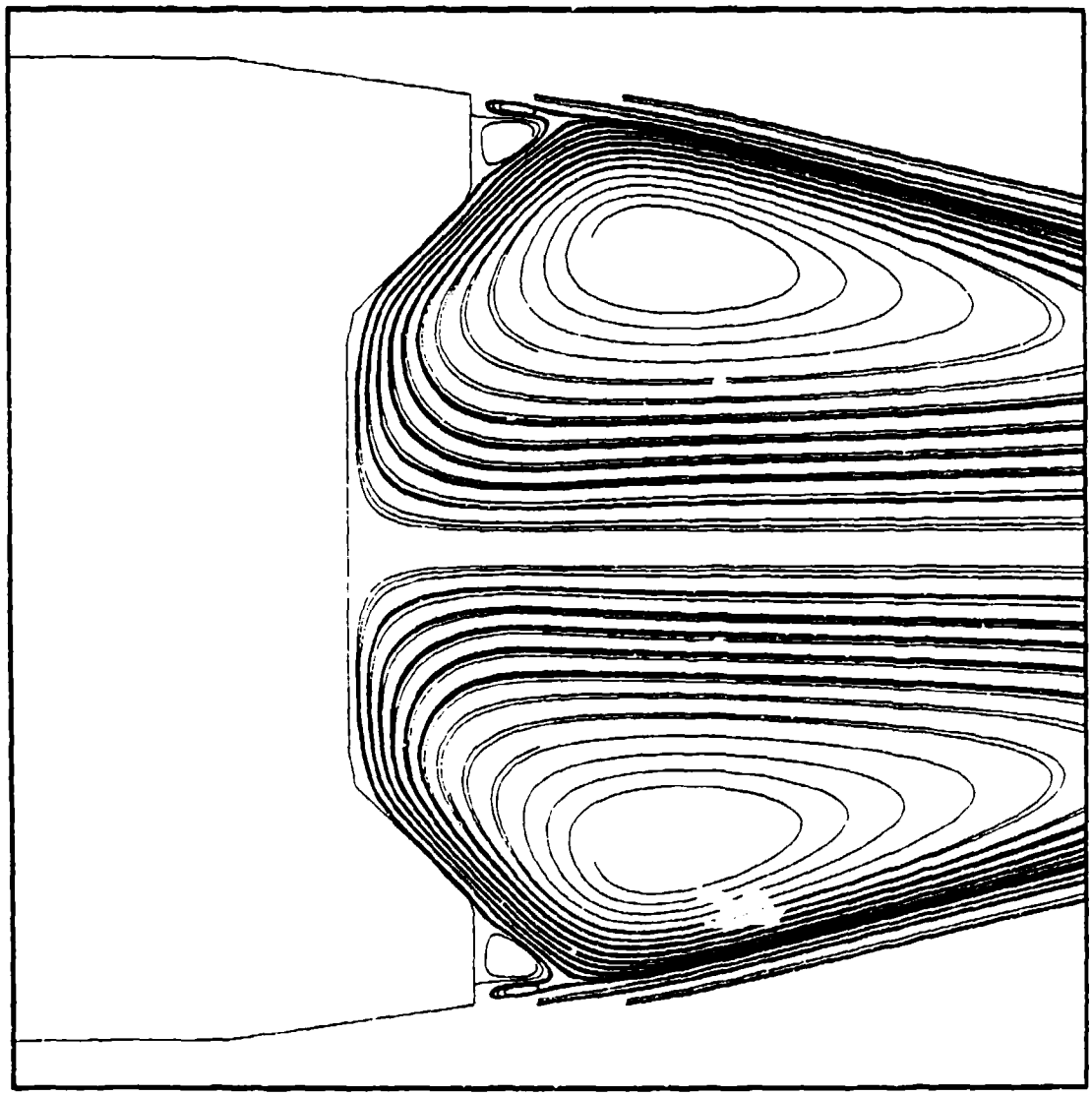

Figure 9a. Particle tracts in the base region, $M_\infty = 1.1$, $\alpha = 0$, (standard base).

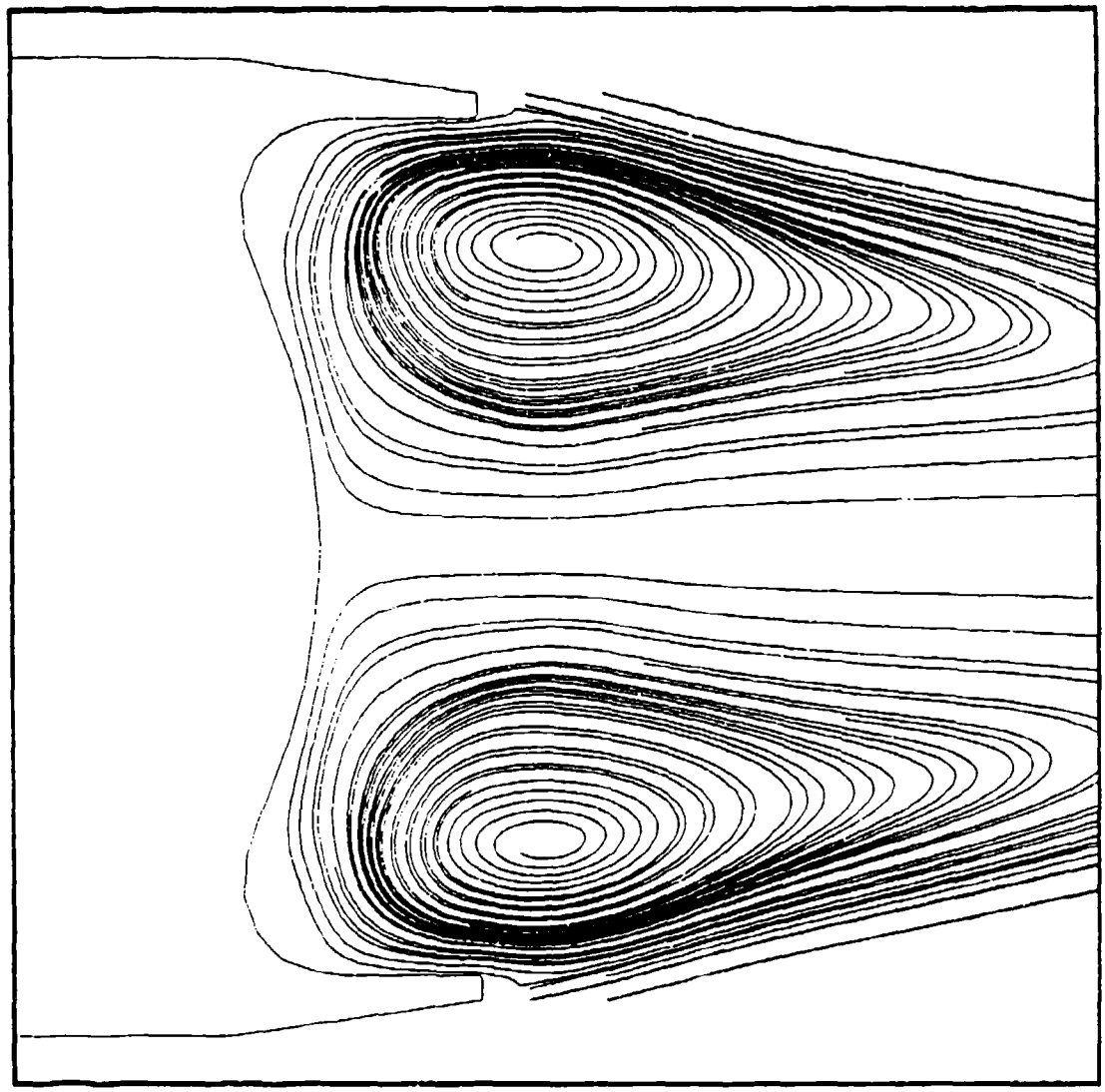

Figure 9b. Particle traces in the base region, M_∞ = 1.1, α 0, (dome base).

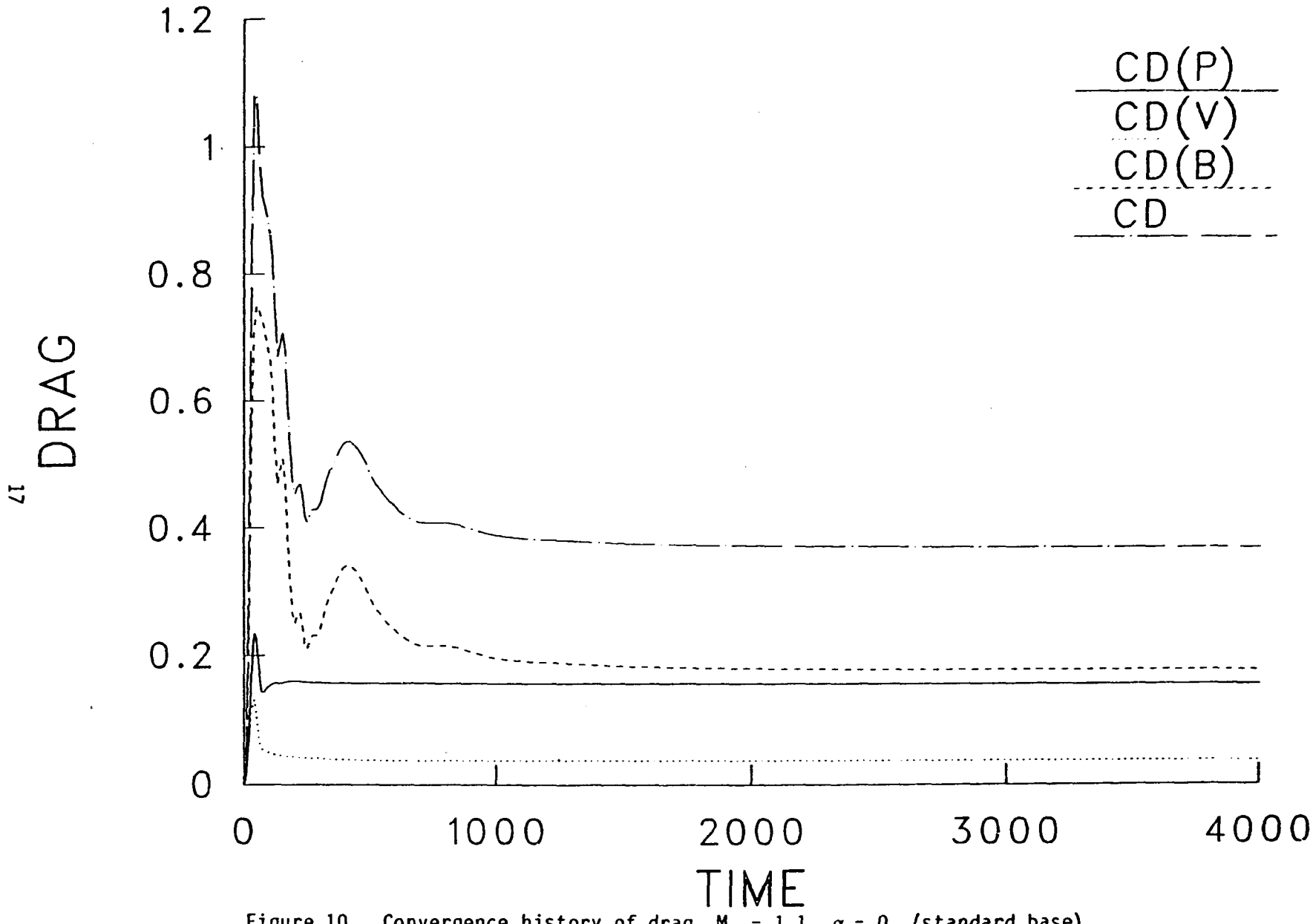

Figure 10. Convergence history of drag, $M_\infty = 1.1$, $\alpha = 0$, (standard base).

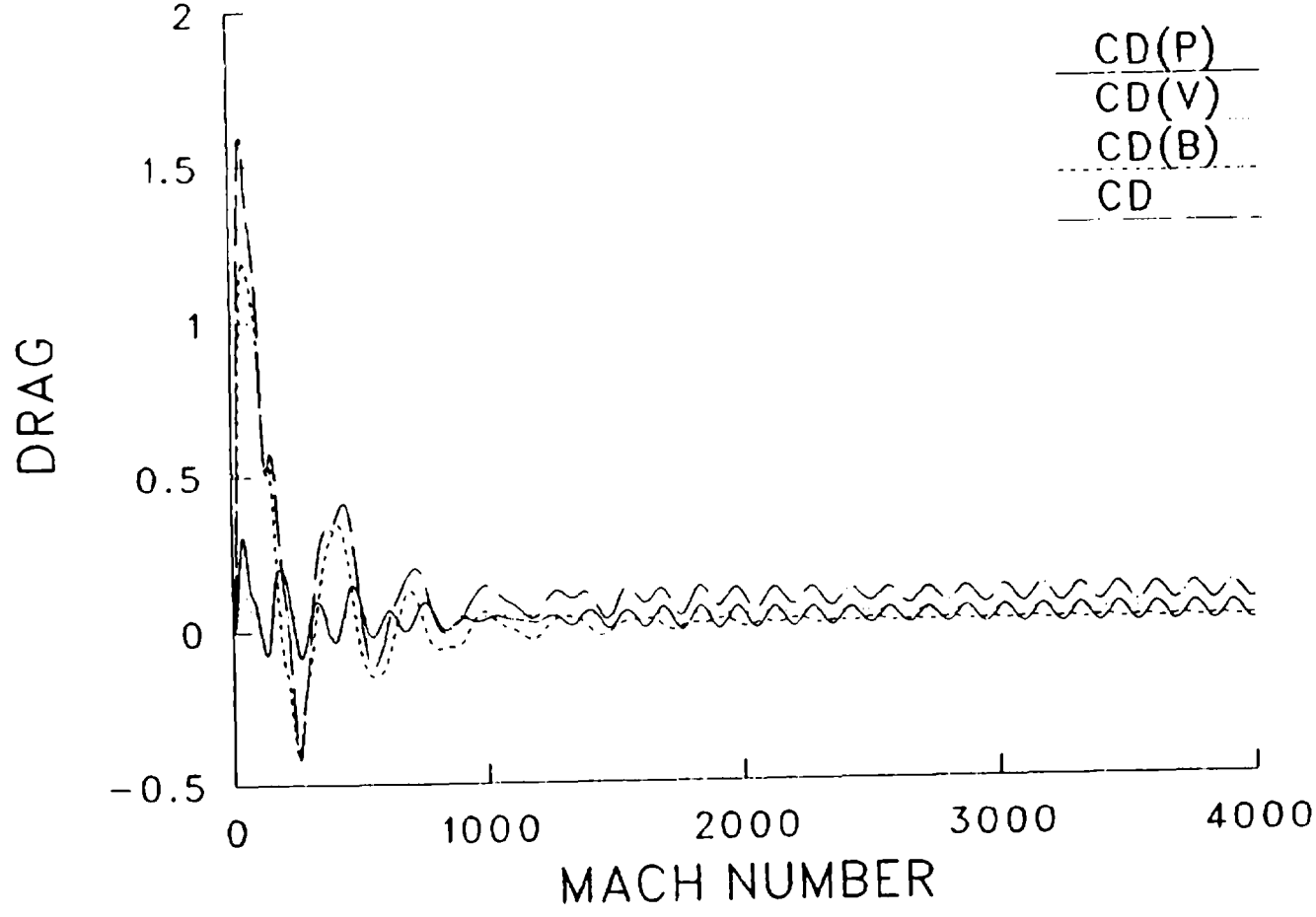

Figure 11. Convergence history of drag, $M_\infty = 0.8$, $\alpha = 0$, (standard base).

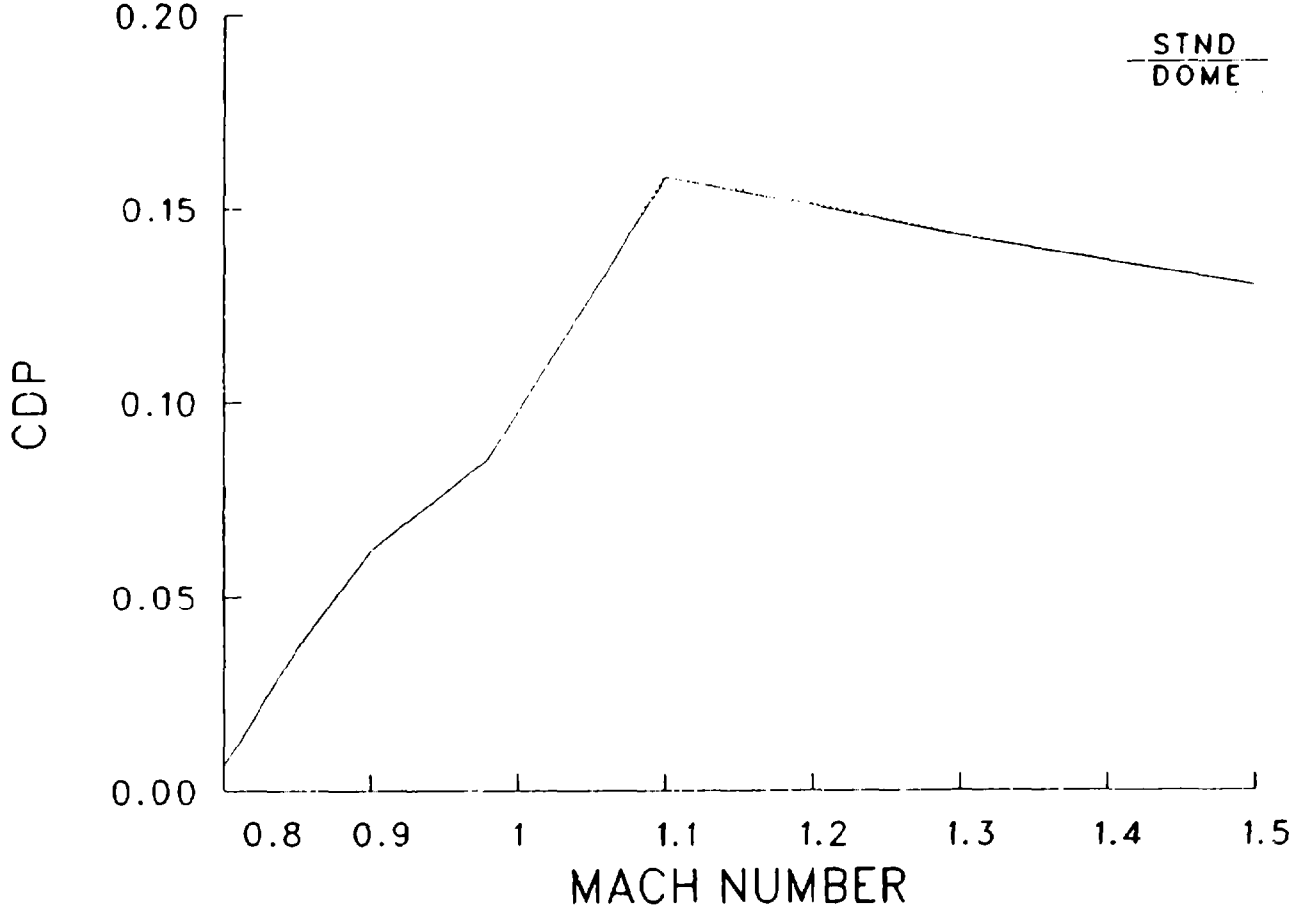

Figure 12. Variation of pressure drag with Mach number, $\alpha = 0$.

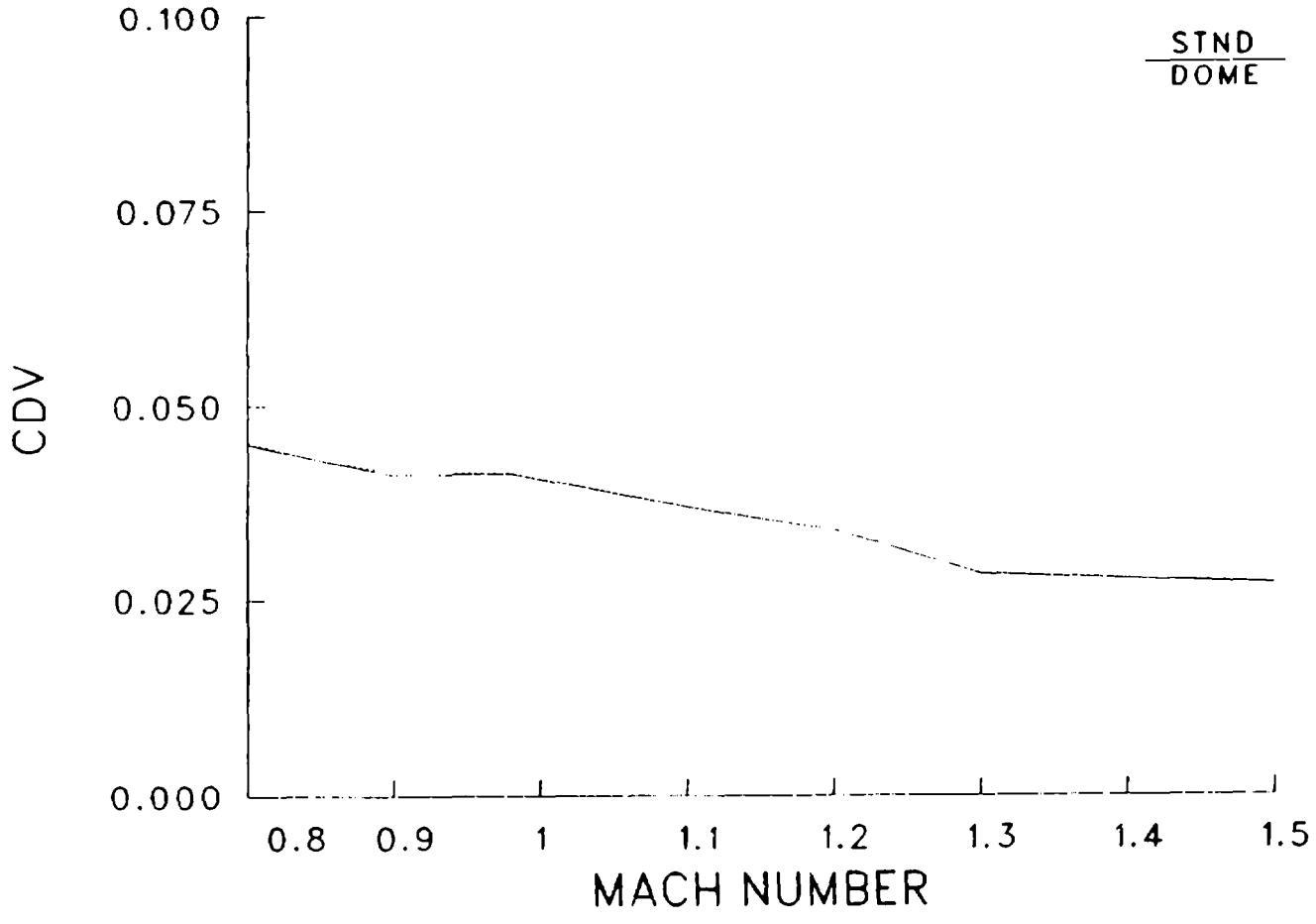

Figure 13. Variation of viscous drag with Mach number, $\alpha = 0$.

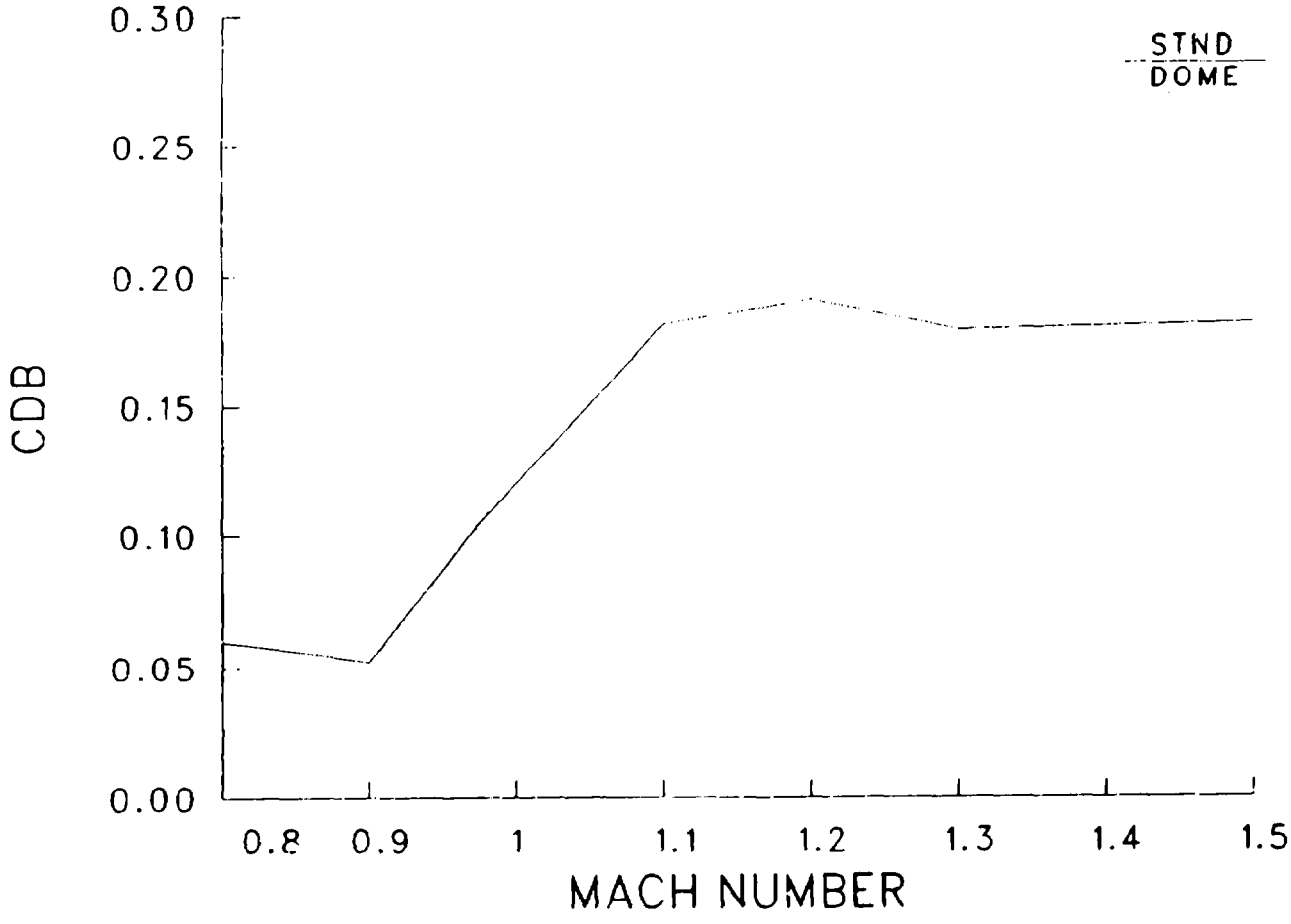

Figure 14. Variation of base drag with Mach number, $\alpha = 0$.

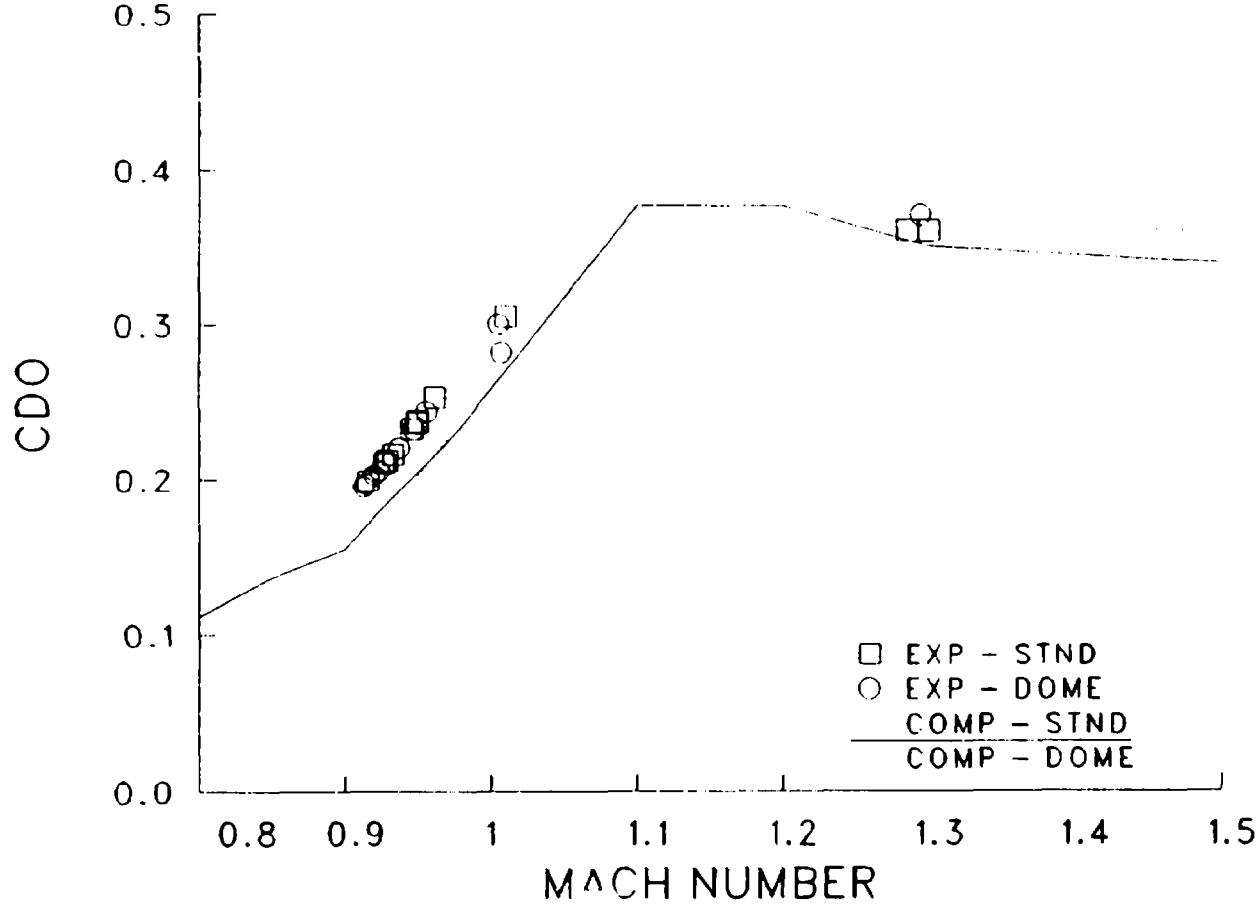

Figure 15. Variation of total drag with Mach number, $\alpha = 0$.

REFERENCES

1. D'Amico, W.P., "Transonic Range Testing of the 155mm M825 Projectile with Standard and Dome Steel Bases," US Army Ballistic Research Laboratory, Aberdeen Proving Ground, Maryland, report to be published.

2. Nietubicz, C.J., Pulliam, T.H., and Steger, J.L., "Numerical Solution of the Azimuthal-Invariant Navier-Stokes Equations," ARBRL-TR-02227, US Army Ballistic Research Laboratory, Aberdeen Proving Ground, Maryland, March 1980. (AD A085716) (Also see AIAA Journal, Vol. 18, No. 12, December 1980, pp. 1411-1412)

3. Beam, R. and Warming, R.F., "An Implicit Factored Scheme for the Compressible Navier-Stokes Equations," AIAA Paper No. 77-645, June 1977.

4. Sahu, J. and Nietubicz, C.J., "Improved Numerical Prediction of Transonic Flow," Proceedings of the 4th Army Conference on Applied Mathematics and Computing, Cornell University, May 1986.

5. Pulliam, T.H. and Steger, J.L., "On Implicit Finite-Difference Simulations of Three-Dimensional Flow," AIAA Journal, Vol. 18, No. 2, February 1980, pp. 159-167.

6. Sahu, J., Nietubicz, C.J., and Steger, J.L., "Navier-Stokes Computations of Projectiles Base Flow with and without Base Injection," ARBRL-TR-02532, US Army Ballistic Research Laboratory, Aberdeen Proving Ground, Maryland, November 1983. (AD A135738) (Also see AIAA Journal, Vol. 23, No. 9, September 1985, pp. 1348-1355)

7. Baldwin, B.S. and Lomax, H., "Thin-Layer Approximation and Algebraic Model for Separated Turbulent Flows," AIAA Paper No. 78-257, 1978.

8. Chow, W.L., "Improvement on Numerical Computations of the Thin-Layer Navier-Stokes Equation with Emphasis on the Turbulent Base Pressure of a Projectile in Transonic Flight Condition," Contract Report No. DAAG29-81-D-0100, U.S. Army Ballistic Research Laboratory, Aberdeen Proving Ground, Maryland, November 1985.

9. Nietubicz, C.J., Heavey, K.R., and Steger, J.L., "Grid Generation Techniques for Projectile Configurations," Proceedings of the 1982 Army Numerical Analysis and Computers Conference, ARO Report 82-3, February 1982.

LIST OF SYMBOLS

a	=	speed of sound
D	=	body diameter
e	=	total energy per unit volume/$\rho_\infty a_\infty^2$
$\hat{E}$, $\hat{G}$,	=	flux vector of transformed Navier-Stokes equations
h	=	time step
$\hat{H}$	=	n-invariant source vector
J	=	Jacobian of transformation
M	=	Mach number
p	=	pressure/$\rho_\infty a_\infty^2$
$\hat{q}$	=	dependent variables
Re	=	Reynolds number, $\rho_\infty a_\infty D/\mu_\infty$
$\hat{S}$	=	viscous flux vector
t	=	physical time
u, v, w	=	Cartesian velocity components/a_∞
x, y, z	=	physical Cartesian coordinates

Greek Symbols

α	=	angle of attack
μ	=	coefficient of viscosity/μ_∞
ξ, η, ζ	=	transformed coordinates in axial, circumferential and radial directions
ρ	=	density/ρ_∞

DISTRIBUTION LIST

No. of Copies	Organization
12	Administrator Defense Technical Info Center ATTN: DTIC-FDAC Cameron Station, Bldg 5 Alexandria, VA 22304-6145
1	HQDA DAMA-ART-M Washington, DC 20310
1	Commander US Army Materiel Command ATTN: AMCDRA-ST 5001 Eisenhower Avenue Alexandria, VA 22333-0001
3	Commander US Army Armament Research, Development and Engineering Center ATTN: SMCAR-MSI SMCAR-LCA-F/Klein Hudgins Dover, NJ 07801-5001
1	Commander US Army Armament Research, Development and Engineering Center ATTN: SMCAR-TDC Dover, NJ 07801-5001
1	Commander US AMCCOM ARDEC CCAC Benet Weapons Laboratory ATTN: SMCAR-CCB-TL Watervliet, NY 12189-4050
1	Commander US Army Armament, Munitions and Chemical Command ATTN: AMSMC-IMP-L Rock Island, IL 61299-7300
1	Commander US Army Aviation Systems Command ATTN: AMSAV-ES 4300 Goodfellow Blvd. St. Louis, MO 63120-1798
1	Director US Army Aviation Research and Technology Activity Ames Research Center Moffett Field, CA 94035-1099
10	C.I.A OIR/DB/Standard GE47 HQ Washington, DC 20505
1	Commander US Army Communications - Electronics Command ATTN: AMSEL-ED Fort Monmouth, NJ 07703-5301
1	Commander CECOM R&D Technical Library ATTN: AMSEL-IM-L (Reports Section) B.2700 Fort Monmouth, NJ 07703-5000
1	Commander US Army Missile Command Research, Development, and Engineering Center ATTN: AMSMI-RD Redstone Arsenal, AL 35898-5230
1	Director US Army Missile and Space Intelligence Center ATTN: AIAMS-YDL Redstone Arsenal, AL 35898-5500
1	Commander US Army Tank Automotive Command ATTN: AMSTA-TSL Warren, MI 48397-5000
1	Director US Army TRADOC Analysis Center ATTN: ATOR-TSL White Sands Missile Range, NM 88002-5502

DISTRIBUTION LIST

No. of Copies	Organization
2	Commander US Naval Surface Weapons Center ATTN: Dr. T. Clare, Code DK20 Dr. F. Moore Dahlgren, VA 22448-5000
1	Commandant US Army Infantry School ATTN: ATSH-CD-CS-OR Fort Benning, GA 31905-5400
1	Commander US Army Development and Employment Agency ATTN: MODE-ORO Fort Lewis, WA 98433-5000
3	Director NASA Ames Research Center ATTN: MS-202-1/Pulliam MS-258-1/Steger Sciff Moffett Field, CA 94035
1	AFWL/SUL Kirtland AFB, NM 87117
1	Air Force Armament Laboratory ATTN: AFATL/DLODL (Tech Info Center) Eglin AFB, FL 32542-5000
2	Sandia National Laboratories ATTN: Dr. W.L. Oberkampf Dr. F. Blottner Division 1636 Albuquerque, NM 87185
1	AEDC Calspan Field Services ATTN: MS 600 (Dr. John Benek) AAFS, TN 37389
1	Virginia Polytechnic Institute & State University ATTN: Dr. Clark H. Lewis Department of Aerospace & Ocean Engineering Blacksburg, VA 24061
1	University of California, Davis Department of Mechanical Engineering ATTN: Prof. H.A. Dwyer Davis, CA 95616
1	Pennsylvania State University Department of Aerospace Engineering ATTN: Dr. G. S. Dulikravich University Park, PA 16802
1	University of Florida Dept. of Engineering Sciences College of Engineering ATTN: Prof. C. C. Hsu Gainesville, FL 32611
1	University of Maryland Department of Aerospace Engineering ATTN: Dr. J.D. Anderson, Jr. College Park, MD 20742
1	University of Illinois at Urbana Champaign Department of Mechanical & Industrial Engineering ATTN: Prof. W. L. Chow Urbana, IL 61801
1	University of Notre Dame Department of Aeronautical & Mechanical Engineering ATTN: Prof. T.J. Mueller Notre Dame, IN 46556
1	University of Texas Department of Aerospace Engineering & Engineering Mechanics ATTN: Dr. D.S. Dolling Austin, Texas 78712-1055

DISTRIBUTION LIST

No. of Copies	Organization
	Aberdeen Proving Ground
	Dir, USAMSAA ATTN: AMXSY-D AMXSY-MP, H. Cohen
	Cdr, USATECOM ATTN: AMSTE-SI-F
	Cdr, CRDC, AMCCOM ATTN: SMCCR-RSP-A SMCCR-MU SMCCR-SPS-IL

USER EVALUATION SHEET/CHANGE OF ADDRESS

This Laboratory undertakes a continuing effort to improve the quality of the reports it publishes. Your comments/answers to the items/questions below will aid us in our efforts.

1. BRL Report Number_____ Date of Report_____

2. Date Report Received_____

3. Does this report satisfy a need? (Comment on purpose, related project, or other area of interest for which the report will be used.)_____

4. How specifically, is the report being used? (Information source, design data, procedure, source of ideas, etc.)_____

5. Has the information in this report led to any quantitative savings as far as man-hours or dollars saved, operating costs avoided or efficiencies achieved, etc? If so, please elaborate._____

6. General Comments. What do you think should be changed to improve future reports? (Indicate changes to organization, technical content, format, etc.)

_____

_____

_____

CURRENT ADDRESS

_____
Name

_____
Organization

_____
Address

_____
City, State, Zip

7. If indicating a Change of Address or Address Correction, please provide the New or Correct Address in Block 6 above and the Old or Incorrect address below.

OLD ADDRESS

_____
Name

_____
Organization

_____
Address

_____
City, State, Zip

(Remove this sheet, fold as indicated, staple or tape closed, and mail.)